SANDIA REPORT
SAND2014-17360
Unlimited Release
Printed September 2014

Hermes III Endpoint Energy Calculation from Photonuclear Activation of ^{197}Au and ^{58}Ni Foils

Christopher T. Parzyck

Prepared by
Sandia National Laboratories
Albuquerque, New Mexico 87185 and Livermore, California 94550

Sandia National Laboratories is a multi-program laboratory managed and operated by Sandia Corporation, a wholly owned subsidiary of Lockheed Martin Corporation, for the U.S. Department of Energy's National Nuclear Security Administration under contract DE-AC04-94AL85000.

Sandia National Laboratories

Issued by Sandia National Laboratories, operated for the United States Department of Energy by Sandia Corporation.

Printed in the United States of America. This report has been reproduced directly from the best available copy.

Available to DOE and DOE contractors from
U.S. Department of Energy
Office of Scientific and Technical Information
P.O. Box 62
Oak Ridge, TN 37831

Telephone: (865) 576-8401
Facsimile: (865) 576-5728
E-Mail: reports@adonis.osti.gov
Online ordering: http://www.osti.gov/bridge

Available to the public from
U.S. Department of Commerce
National Technical Information Service
5285 Port Royal Rd.
Springfield, VA 22161

Telephone: (800) 553-6847
Facsimile: (703) 605-6900
E-Mail: orders@ntis.fedworld.gov
Online order: http://www.ntis.gov/help/ordermethods.asp?loc=7-4-0#online

SAND2014-17360
Unlimited Release
Printed September 2014

Hermes III Endpoint Energy Calculation from Photonuclear Activation of ^{197}Au and ^{58}Ni Foils

Christopher T. Parzyck
Radiation Effects Research Department
Sandia National Laboratories
P.O. Box 5800
Albuquerque, New Mexico 87185-MS1159

Abstract

A new process has been developed to characterize the endpoint energy of HERMES III on a shot-to-shot basis using standard dosimetry tools from the Sandia Radiation Measurements Laboratory. Photonuclear activation readings from nickel and gold foils are used in conjunction with calcium fluoride thermoluminescent dosimeters to derive estimated electron endpoint energies for a series of HERMES shots. The results are reasonably consistent with the expected endpoint voltages on those shots.

ACKNOWLEDGMENTS

The authors would like to thank Dave Vehar and the Radiation Metrology Laboraory for the dosimetry and activation analysis that form the foundation of this work; Ray Thomas and the HERMES III crew for fielding the diagnostics; and Pat Griffin for useful discussions and comments.

CONTENTS

FIGURES

1. FORMULATION

1.1. Measured Activation Data

This report outlines a process to estimate the endpoint energy of the Hermes III photon spectrum, ε, using activation data from gold and nickel foils located in the path of the X-ray beam. Thin foils of ^{197}Au and ^{58}Ni are placed, along with dosimeters, on the X-ray window of the Hermes III accelerator. When the machine is fired electrons are accelerated across a large voltage gap into a converter material. The decelerating electrons in the converter produce Bremsstrahlung radiation which travels out of the machine through an aluminium window and irradiates the foils. These high energy photons interact with the gold and nickel nuclei and cause the emission of photonutrons; the resulting ^{196}Au and ^{57}Ni nuclei are unstable and decay over the course of hours/days. Using measurements of the resulting radioactivity of the foils, as well as knowledge of the spectral shape of the radiation, the endpoint energy of the Bremsstrahlung spectrum (which corresponds to the potential difference across the AK gap) is measured.

The experimentally determined activation of the foil, N_d, is defined as the total number of activated atoms in the given foil after the shot. It is determined by the equation

$$N_d = A\frac{T_{1/2}}{\ln(2)}$$

where A is the measured activity of the foil in Becquerel and $T_{1/2}$ is the half-life of the isotope in seconds. Due to the relatively long half-lives of ^{196}Au and ^{57}Ni (6.17 days and 35.6 hours respectively) the foil activity can be measured roughly a day after irradiation and adjusted to compensate for the passage of time. However, since a non-trivial fraction of the half-lives of ^{196}Au and ^{57}Ni passes between irradiation and measurement, trace amounts of other products in the decay chain are observed in the activated foils. A gamma spectrum analysis is performed on each foil to determine the contribution of the activity from each element/isotope present and accurately calculate the activity due to the presence of ^{196}Au or ^{57}Ni.

1.2. Computed Activation Data

In order to estimate the endpoint energy, ε, a computed activation, N_c is calculated for each value of ε in an anticipated range. N_c is computed using photonuclear cross section data and x-ray spectral data from simulation of the Hermes-III diode. ε is estimated by finding the computed activation which most closely matches the measured activation above. Given a fixed endpoint energy, the activation is computed in two steps. First the total number photon fluence, Φ, incident on the foil is determined by inverting the following equation:

$$D = 1.60 \times 10^{-8}\,\Phi \int_0^{\varepsilon} \psi_\varepsilon(E) R(E)\, dE$$

$$\approx 1.60 \times 10^{-8}\,\Phi \sum_{i=1}^{M} \psi_\varepsilon(E_i) R(E_i) \Delta E_i$$

where D is the total dose from the shot measured using a thermoluminescent dosimeter (TLD) adjacent to the activation foils, Φ is the photon fluence incident on the foil, $\psi_\varepsilon(E)$ is the fractional photon spectrum, and $R(E)$ is a computationally generated response function for the TLD (see section 4 for more information). The numerical factor at the front is the dose conversion factor from MeV/g to rad (as the TLD response functions are calculated in MeV per gram per unit number fluence).

The fractional photon spectrum, $\psi_\varepsilon(E)$, is determined using the 1-D electron–photon transport code, ADEPT. For a given endpoint energy and geometric configuration ADEPT outputs a photon spectrum, $\varphi_\varepsilon(E,\theta)$ in photons/MeV-electron-steradian. $\varphi_\varepsilon(E,\theta)dEd\Omega$ is the number of photons with energy between E and $E + dE$ in an angular bin of solid angle $d\Omega$ (located at an angle θ off the machine axis) produced by a single source electron interacting with the converter material. The fractional spectrum is obtained by normalizing:

$$\psi_\epsilon(E,\theta) = \frac{\phi_\epsilon(E,\theta)}{\int_0^\epsilon \phi_\epsilon(E',\theta)dE'}$$

so that if Φ is the photon fluence in photons/cm^2 at a specified angle θ then $\Phi\ \psi_\varepsilon(E,\theta)dEdA$ gives the total number of photons crossing a patch of area dA located at an angle θ with energies between E and $E + dE$. For any given shot, the value of θ is fixed by the location of the activation foil and TLD packet with respect to the machine centerline.

Given the photon fluence, Φ, the number of activated atoms, N_c, is then calculated using cross section data for the (γ,n) reaction obtained from the experimental nuclear reaction database, EXFOR.

$$N_c = 10^{-27}\, N\, \Phi \int_0^\epsilon \psi_\epsilon(E)\sigma(E)\, dE$$

$$\approx 10^{-27}\, N\, \Phi \sum_{i=1}^{M} \psi_\epsilon(E_i)\sigma(E_i)\Delta E_i$$

where N is the total number of atoms in the foil, σ is the (γ,n) cross section in mbarn, and the numerical factor is the conversion from mbarn to cm^2. The value of N is determined by careful measurement of the masses of the foils.

In summary, for a given value of the endpoint energy ε, a prediction for the number of activated atoms in an irradiated foil is given by

$$N_c(\epsilon) = \frac{10^{-27}\, N D\, \int_0^\epsilon \psi_{\epsilon_0}\sigma\, dE}{1.60 \times 10^{-8}\, \int_0^\epsilon \psi_\epsilon R\, dE}$$

$$\approx 6.25 \times 10^{-20} N D \frac{\sum_{i=1}^{M} \psi_\epsilon(E_i)\sigma(E_i)\, \Delta E_i}{\sum_{i=1}^{M} \psi_\epsilon(E_i) R(E_i)\, \Delta E_i}$$

To extract an estimate for the endpoint energy itself, N_c is computed for nine values of ε in the range of 8.55 to 19.05 MeV. Due to the spectral shape of the Hermes–III source, N_c (ε) is monotonic increasing on this interval, and thus can be inverted to obtain a plot of ε(N_c). The endpoint energy of the shot is then estimated as ε(N_d), where N_d was the measured activation obtained by the process described in section 1.1. For simplicity, $\varepsilon(N_d)$, was computed using linear interpolation of the data obtained from computing N_c (ε) for the following values of ε: 8.56, 9.45, 10.45, 11.55, 12.76, 14.11, 15.59, 17.23, and 19.05 MeV.

Shot #	Foil Mass (g)	Activity (^{196}Au) (Bq)	Activity (^{57}Ni) (Bq)	Dose (rad)	Angle (degrees)
9731	0.1940	137.34	68.08	107000	65.00
9737	0.1938	-	-	7577	0.00
9756	0.1987	1.70	-	20150	0.00
9757	0.1951	37.53	50.24	45770	0.00
9758	0.1955	35.74	36.27	47200	0.00
9759	0.1939	3.09	-	22830	0.00
9760	0.1951	1.37	-	24600	0.00
9761	0.1972	29.75	38.81	42520	0.00

Figure 1 Activity and dose data for HERMES shots.

2. ERROR ANALYSIS

Basic error propagation techniques are used to derive confidence bounds on the above estimate of the endpoint energy, ε. Three sources of experimental error are factored into the uncertainty computation: the uncertainty in the dose data, δD, the uncertainty in the measured activation data, δN_d, and the uncertainty in the (γ,n) cross section data, $\delta\sigma_i = \delta(\sigma(E_i))$. Since both of the quantities D and σ are explicitly factored into the calculation of N_c the corresponding uncertainty, δN_c ,can be computed via the standard error propagation formula:

$$\delta N_c = \sqrt{\left(\frac{\partial N_c}{\partial D}\delta D\right)^2 + \sum_{i=1}^{M}\left(\frac{\partial N_c}{\partial \sigma_i}\delta\sigma_i\right)^2}$$

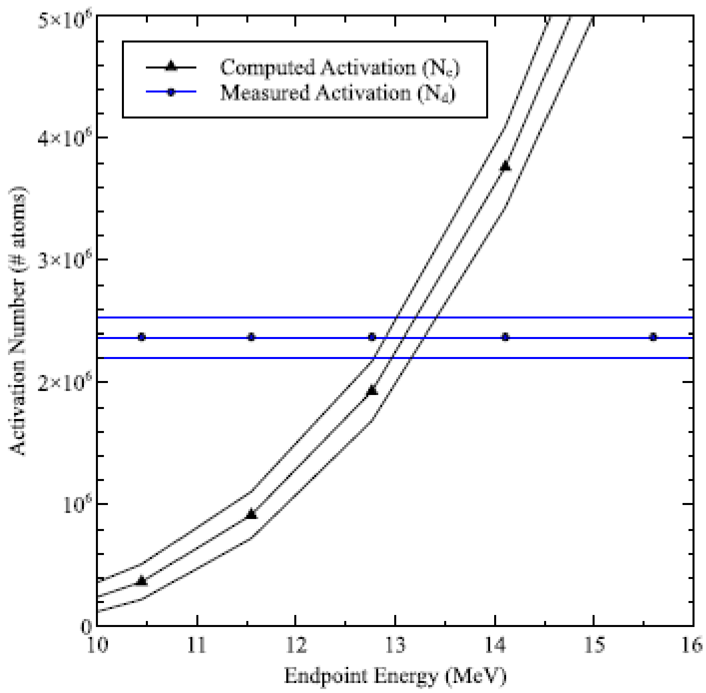

Figure 2 Values of N_d and N_c for shot 9759 with 1 sigma confidence intervals. A dose uncertainty of $\delta D/D$ = 6% and an activity uncertainty of $\delta Nd/Nd$ = 7% were assumed.

On the other hand, the effects of δNc and δNd on the estimation of the endpoint energy are slightly more difficult to quantify. Consider the graph of the computed and measured activations ($N_c(\varepsilon)\pm\delta N_c(\varepsilon)$ and $N_d\pm\delta N_d$ respectively) in figure 1. The effect of computing the endpoint energy using the linear interpolation scheme in the previous section is the same as finding the x coordinate on this graph of the intersection point of Nd and $N_c(\varepsilon)$. To produce a lower confidence bound on the endpoint energy the x coordinate of the intersection between the lower confidence bound on the activation data (N_d-δN_d) and the upper confidence bound of the computed activation ($N_c(\varepsilon)+\delta N_c(\varepsilon)$). On the chart this is the lower leftmost of the five intersection points. Similarly the intersection of $N_d+\delta N_d$ and $N_c(\varepsilon)$-$\delta N_c(\varepsilon)$, i.e. the top rightmost intersection point, is used to give an upper confidence bound on the estimate of the endpoint energy.

3. CROSS SECTION DATA PROCESSING

The cross section data for the (γ,n) reaction was obtained by consolidating a number of datasets from the EXFOR database. The datasets for each element were consolidated and interpolated using the smoothing spline algorithm of de Boor [1]. The smoothing aspect of the algorithm acts roughly as a low pass filter with effective frequency response

$$\phi(\omega) = 1/(1+(\omega/\omega_{0.5})^4)$$

where $\omega_{0.5}$ is the 50% attenuation frequency. For both the nickel and gold cross sections $\omega_{0.5}$ is set such that the 50% attenuation period, $2\pi/\omega_{0.5}$, is 0.5 MeV. This is because 0.5 MeV is roughly the width of the energy bins used in the spectral data in the region where the cross sections are non–vanishing: $\Delta E_i \approx 0.5$MeV for $8 < E_i < 20$ MeV.

Each of the selected cross section datasets reported one sigma uncertainties for each of the data point. In order to propagate the uncertainties in the datasets into the interpolated data the method introduced by Enting et al. in [2] was used. However, for the gold data in the high energy regime, > 12MeV, there was only data set which provided cross section data. For each of these points a relative error of 10% was reported. Since it was unclear if this error was predominately systematic or random and the error propagation method previously mentioned treats all errors as random (leading to a calculated uncertainty of much less then 10% for some points) the choice was made to replace the uncertainties furnished by the algorithm with constant 10% errors for ^{197}Au data above 12 MeV. Plots of the original cross section data, as well as the smoothed/interpolated data for both elements are included as figures 2 through 5.

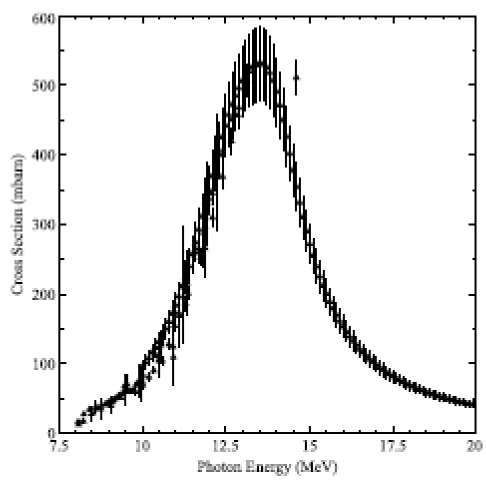

Figure 3 EXFOR (γ,n) cross section data for ^{197}Au.

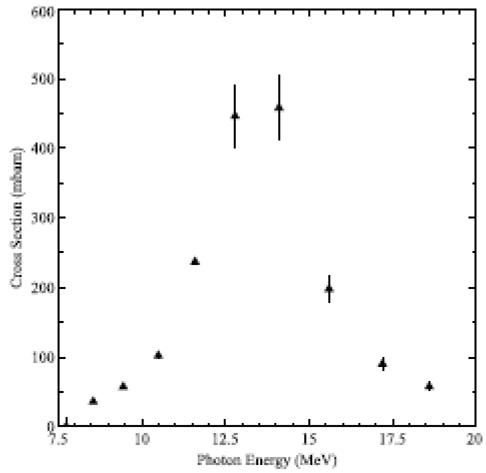

Figure 4 Smoothing spline interpolation for ^{197}Au.

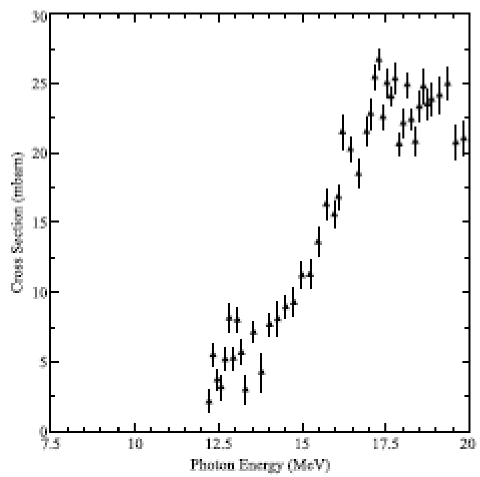

Figure 5 EXFOR (*γ,n*) cross section data for ^{58}Ni.

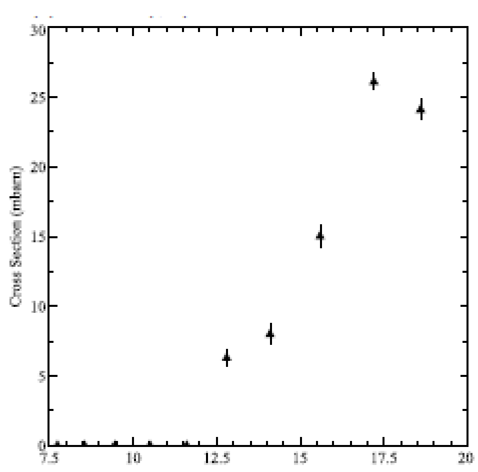

Figure 6 Smoothing spline interpolation for ^{58}Ni.

4. TLD RESPONSE FUNCTIONS

The TLD response function data, *R(E)*, was derived from adjoint mode ADEPT calculations. ADEPT, a one dimensional photon–electron transport code, running in adjoint mode outputs the dose deposited per unit number fluence in a TLD (for a set thickness and material composition of the dosimeter) as a function of incoming photon energy. This data is then interpolated (using MATLAB's build in hermite polynomial interpolation routine, `pchip`) to the same energy grid as the spectral data. It should be mentioned that in the ADEPT calculations the photons were assumed to be normally incident on the TLD surface, although in some shots the TLD's were placed off machine axis, so the incident photons were not necessarily normally incident to the dosimetry. The effects of changing this angle of incidence of were studied, and it was found that for an assumed angle of 40° off normal the predicted endpoint energies were between 0.33 and 1.35 MeV higher than calculations with normally incident photons.

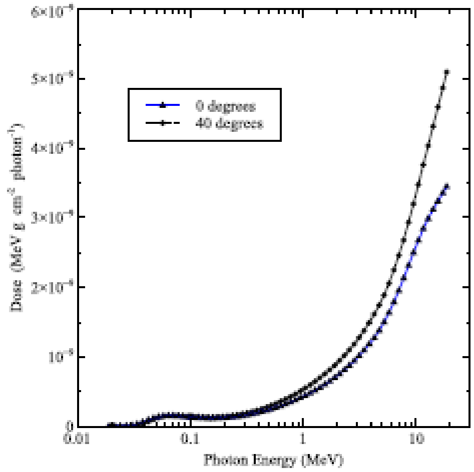

Figure 7 TLD response function for normally incident and off-normal incident photons.

5. RESULTS AND CONCLUSIONS

Results of the above analysis for a number of Hermes–III shots are included in tables 1 through 4. Table 4 contains a comparison of the predicted endpoint energies using the gold and nickel activation data for those shots on which both foils were processed. It indicates a good agreement between the nickel and gold results (modulo the uncertainties in the endpoint energy estimates). In each case that was comparable, the difference between the predicted endpoint energies (ε_{Au} and ε_{Ni}), was less than 1 MeV and in most cases the uncertainties in the estimates of the endpoint energy, $\delta\varepsilon$, were roughly 0.5 MeV. Only in shot 9761 was the discrepancy between ε_{Au} and ε_{Ni} much larger than either of the computed uncertainties. This agreement between the predicted endpoint energies using the two different foil materials is encouraging, and seems to indicate that the cross section data for the (γ,n) reaction is reasonable.

Shot #	ϵ_- MeV	ϵ MeV	ϵ_+ MeV
9731	>19	>19	>19
9737	-	-	-
9756	11.64	11.90	12.19
9757	17.63	18.18	18.81
9758	16.93	17.38	17.93
9759	12.42	12.74	12.96
9760	10.91	11.27	11.64
9761	16.84	17.27	17.82

Figure 8 Predicted endpoint energies (ε) from Au activation data with upper/lower confidence bounds (ε+ and ε- respectively).

Shot #	ϵ_- MeV	ϵ MeV	ϵ_+ MeV
9731	16.53	16.76	17.02
9737	-	-	-
9756	-	-	-
9757	18.39	18.68	19.01
9758	17.50	17.71	17.96
9759	-	-	-
9760	-	-	-
9761	17.87	18.11	18.39

Figure 9 Predicted endpoint energies (ε) from Ni activation data with upper/lower confidence bounds (ε+ and ε- respectively).

Shot #	Δ MeV	$\delta\epsilon$ (^{167}Au) MeV	$\delta\epsilon$ (^{58}Ni) MeV
9731	-	-	0.246
9737	-	-	-
9756	-	0.276	-
9757	0.505	0.591	0.311
9758	0.338	0.500	0.227
9759	-	0.272	-
9760	-	0.362	-
9761	0.842	0.486	0.261

Figure 10 Comparison of predicted endpoint energies from Ni and Au activation data. Δ is the difference between the gold and nickel predictions: $\Delta = |\varepsilon_{Au} - \varepsilon_{Ni}|$. $\delta\varepsilon$ is roughly the uncertainty in the endpoint energy: $\delta\varepsilon = 0.5(\varepsilon+ - \varepsilon-)$.

6. REFERENCES

[1] Carl De Boor. A practical guide to splines; rev. ed.Applied mathematical sciences. Springer, Berlin, 2001.

[2] D. M. Etheridge I. G. Enting, C. M. Trudinger. Propagating data uncertainty through smoothing spline fits. *Tellus* B, 2011.

DISTRIBUTION

1	MS0899	Technical Library	9536 (electronic copy)

Sandia National Laboratories